Journal of Solid State Chemistry 183 (2010) 2196–2204

Contents lists available at ScienceDirect

Journal of Solid State Chemistry

journal homepage: www.elsevier.com/locate/jssc

Synthesis and structural characterisation using Rietveld and pair distribution function analysis of layered mixed titanium–zirconium phosphates

Victoria A. Burnell [a], Jennifer E. Readman [a], Chiu C. Tang [b], Julia E. Parker [b], Stephen P. Thompson [b], Joseph A. Hriljac [a,*]

[a] School of Chemistry, The University of Birmingham, Edgbaston, Birmingham B15 2 TT, UK
[b] Diamond Light Source Ltd., Diamond House, Harwell Science and Innovation Campus, Didcot, Oxfordshire OX11 0DE, UK

ARTICLE INFO

Article history:
Received 5 April 2010
Received in revised form
13 July 2010
Accepted 17 July 2010
Available online 24 July 2010

Keywords:
Layered phosphates
Titanium
Zirconium
Pair distribution function analysis
Solid solution

ABSTRACT

Crystalline metal (IV) phosphates with variable zirconium-to-titanium molar ratios of general formula $(Ti_{1-x}Zr_x)(HPO_4)_2 \cdot H_2O$ have been prepared by precipitation of soluble salts of the metals with phosphoric acid and heating the amorphous solids in 12 M H_3PO_4 in an autoclave. The new materials are structurally characterised by Rietveld analysis of synchrotron X-ray powder diffraction data and pair distribution function (PDF) analysis of high energy synchrotron X-ray total scattering data. A broad range of zirconium–titanium phosphate solid solutions were formed showing isomorphous substitution of titanium by zirconium in the α-titanium phosphate lattice and vice versa for titanium substitution into the α-zirconium phosphate lattice. In both cases the solubility is partial with the coexistence of two substituted phases observed in samples with nominal compositions between the solubility limits.

1. Introduction

The ion exchange properties of the insoluble acid salts of tetravalent metal ions have been known for many years [1–6]; however there has been a renewed interest in them owing to their favourable ion exchange properties and high resistance towards temperature and radiation, making them ideal for use in the nuclear industry. The investigation of mixed compounds of this and other types is also of interest because of the potential for fine tuning of the ion-exchange selectivity through chemical control. In addition to Ti and Zr, isomorhous solids are also known based on Pb [7], Sn [8] and Ge [7,9].

$Ti(HPO_4)_2 \cdot H_2O$ (designated α-TiP) has the same layer structure as α-zirconium phosphate (α-ZrP) with approximately the same interlayer distance of 7.56 Å, Fig. 1 [10]. It does, however, have denser metal-phosphate layers due to the smaller ionic radius of Ti, hence the intralayer environment for, e.g, cation binding, is different. It is of interest to attempt the preparation of mixed zirconium–titanium phosphates for two main reasons. The first is to determine whether the ion exchange properties could be altered and controlled in this manner, the second is to stabilise the Ti-rich samples as it is known that the phosphate groups are more readily hydrolysed [5].

The first reported attempt to prepare a few mixed zirconium–titanium phosphates was by Clearfield and Frianeza [5] via precipitation of the metals from solution with phosphoric acid and refluxing of the amorphous solids in concentrated H_3PO_4. Later, Farfán-Torres et al. [11] attempted to prepare mixed zirconium–titanium phosphates by sol–gel processing, using $Zr[O(CH_2)_2CH_3]_4$ and $Ti[OCH(CH_3)_2]_4$ as precursors, which were hydrolysed with phosphoric acid to form amorphous solids that were then crystallised via reflux in 9 M phosphoric acid. A third preparative method has been reported involving slow phosphoric acid precipitation of the flurocomplexes of zirconium and titanium formed in HF aqueous solution followed by crystallisation by refluxing in 12 M phosphoric acid [12]. These previous studies had either limited or unproven success at synthesising the full range of mixed metal solid solutions and often lead to poorly crystalline solids. It has also been hypothesised that the structures change with the changing metal ratios, however no structural refinements have been carried out on any of the products to prove this. In this paper we present our attempts of the synthesis of the mixed zirconium–titanium phosphates of composition $Ti_{1x}Zr_x(HPO_4)_2 \cdot H_2O$ where $x=0$–1, by an alternative hydrothermal crystallisation route. The crystal structures of the single-phase products were determined to high precision by Rietveld refinements of high resolution synchrotron X-ray powder diffraction data which also allowed an investigation into the structure changes caused by varying metal ratios. Pair distribution function analysis has also been employed to determine whether the solid

* Corresponding author. Fax: +44 121 414 4403.
E-mail address: j.a.hriljac@bham.ac.uk (J.A. Hriljac).

0022-4596/$ - see front matter © 2010 Elsevier Inc. All rights reserved.
doi:10.1016/j.jssc.2010.07.028

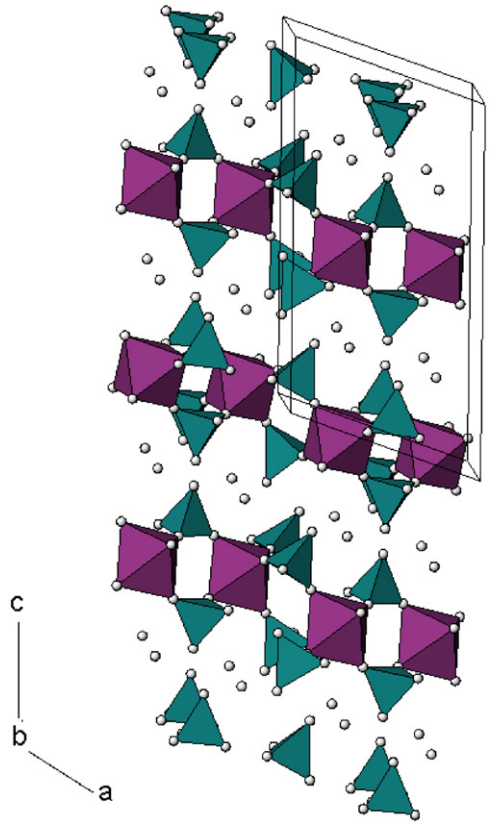

Fig. 1. Polyhedral representation of the α-TiP ($Ti(HPO_4)_2 \cdot H_2O$) structure with phosphate tetrahedra in green, titanium octahedra in purple and oxygen atoms as small spheres. The water molecules sit between the layers. Approximate unit cell parameters of $a=8.63$, $b=5.01$, $c=16.19$ Å and $\beta=110.21^\circ$. (For interpretation of the references to colour in this figure legend, the reader is referred to the web version of this article.)

solutions have a random or locally ordered metal distribution, this information is lacking in Rietveld refinements that only model average long-range structures.

2. Materials and methods

2.1. Sample preparation

2.1.1. α-TiP

The experimental procedure was similar to that previously reported by Clearfield and Frianeza [5]. The crude gel was prepared by the addition of 1 M $TiCl_4$ solution to 50 ml H_3PO_4 (4 M). The solution was stirred overnight at room temperature. The crude gel was collected by filtration, washed with deionised water, reslurried with 12 M H_3PO_4 and heated to 150 °C in a 25 ml autoclave for 1 week. The resultant product was collected by centrifugation and washed by reslurrying the product with deionised water and centrifuging until the pH of the supernatant reached approximately 4 to ensure it was free of H_3PO_4.

2.1.2. α-ZrP

The synthesis is as described above for TiP, except that the crude gel was formed by the addition of 1 M zirconyl chloride solution to 4 M H_3PO_4. The zirconyl chloride solution had been previously prepared by dissolving zirconyl chloride powder in 1 M HCl.

2.1.3. Coprecipitates

The first part of the experimental procedure was similar to that previously reported by Clearfield and Frianeza [5]. Solutions of 1 M titanium tetrachloride and zirconyl chloride were firstly prepared using 1 M acetic acid and 1 M HCl solutions, respectively. These were mixed together in stoichiometric amounts to give the desired Zr/Ti ratios. Then 50 ml of 4 M H_3PO_4 were added to each of these mixtures and they were stirred overnight. The crude gels were collected by filtration and reslurried with 12 M H_3PO_4 before being heated at 150 °C for 1 week in a 23 ml autoclave. The resultant products were collected by centrifugation and washed by reslurrying the products with deionised water and centrifuging until the pH of the supernatant reached approximately 4 indicating that the excess acid was no longer present.

2.2. Characterisation

X-ray powder diffraction data for routine phase analysis were collected in-house on a Bruker D5000 diffractometer in flat plate transmission mode with samples held between tape and operating with Ge-monochromated radiation of wavelength 1.5406 Å in θ–2θ geometry and using a Braun position sensitive detector. High resolution synchrotron X-ray powder diffraction data for Rietveld refinements were collected at Beamline I11 at the Diamond Light Source, UK with the 45-crystal MAC array detector and using radiation of wavelength 0.82668(6) Å based on calibration with a silicon standard. The design and technical details of the beamline are given elsewhere [13,14]. Samples were packed into thin-walled 0.5 mm diameter glass capillaries and typical count times were 45 min; data were binned in 0.005° steps in 2θ. Refinements were performed with the GSAS program package [15]. For the pair

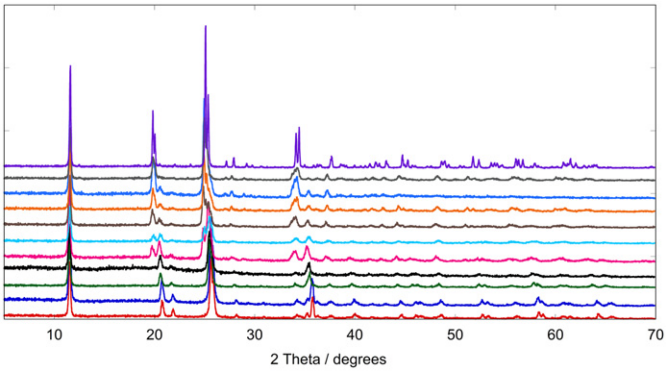

Fig. 2. Overlaid laboratory X-ray powder diffraction scans of the Zr/Ti phosphates. The pattern of the Ti end-member is at the bottom, Zr at the top and successive 0.1 composition increments between them.

Table 1
Chemical compositions of the mixed zirconium–titanium phosphates as determined by XRF.

Nominal formula	Mass % Ti (relative)	Mass % Zr (relative)	Measured formula
$Ti_{0.9}Zr_{0.1}(HPO_4)_2 \cdot H_2O$	32.8	8.3	$Ti_{0.88}Zr_{0.12}(HPO_4)_2 \cdot H_2O$
$Ti_{0.8}Zr_{0.2}(HPO_4)_2 \cdot H_2O$	27.3	17.5	$Ti_{0.75}Zr_{0.25}(HPO_4)_2 \cdot H_2O$
$Ti_{0.7}Zr_{0.3}(HPO_4)_2 \cdot H_2O$	24.3	22.3	$Ti_{0.68}Zr_{0.32}(HPO_4)_2 \cdot H_2O$
$Ti_{0.6}Zr_{0.4}(HPO_4)_2 \cdot H_2O$	21.9	34.0	$Ti_{0.55}Zr_{0.45}(HPO_4)_2 \cdot H_2O$
$Ti_{0.5}Zr_{0.5}(HPO_4)_2 \cdot H_2O$	21.9	35.9	$Ti_{0.53}Zr_{0.47}(HPO_4)_2 \cdot H_2O$
$Ti_{0.4}Zr_{0.6}(HPO_4)_2 \cdot H_2O$	21.9	45.2	$Ti_{0.48}Zr_{0.52}(HPO_4)_2 \cdot H_2O$
$Ti_{0.3}Zr_{0.7}(HPO_4)_2 \cdot H_2O$	21.9	48.2	$Ti_{0.46}Zr_{0.54}(HPO_4)_2 \cdot H_2O$
$Ti_{0.2}Zr_{0.8}(HPO_4)_2 \cdot H_2O$	21.9	49.2	$Ti_{0.46}Zr_{0.54}(HPO_4)_2 \cdot H_2O$
$Ti_{0.1}Zr_{0.9}(HPO_4)_2 \cdot H_2O$	3.2	36.3	$Ti_{0.14}Zr_{0.86}(HPO_4)_2 \cdot H_2O$

distribution function analysis the samples were packed in kapton capilliaries and the data collected at Station 11-ID-B at the APS using a wavelength of 0.1370 Å and a GE amorphous Si detector. FIT2D [16] was employed to integrate the data, PdfgetX2 [17] to process it and PDFGui [18] for the refinements. The Zr:Ti molar ratios of the samples were determined by X-ray flourescence (XRF) using a Bruker S8 Tiger high-end wavelength dispersive X-ray fluorescence (WDXRF) spectrometer.

3. Results and discussion

3.1. Laboratory X-ray powder diffraction (XRD)

Based on the in-house XRD analysis all of the products were obtained as crystalline materials. Comparison of the data obtained for the mixed Zr/Ti series as well as the pure TiP and ZrP end-members are shown in Fig. 2. It can be seen that many of the XRD

Table 2
Structural parameters with estimated standard deviations for the single-phase members of the series from the Rietveld refinements.

	α-TiP	$Ti_{0.9}Zr_{0.1}(HPO_4)_2 \cdot H_2O$	$Ti_{0.8}Zr_{0.2}(HPO_4)_2 \cdot H_2O$	$Ti_{0.7}Zr_{0.3}(HPO_4)_2 \cdot H_2O$	$Ti_{0.1}Zr_{0.9}(HPO_4)_2 \cdot H_2O$	α-ZrP
a/Å	8.63267(6)	8.65991(12)	8.69672(13)	8.7156(3)	9.0048(2)	9.06336(2)
b/Å	5.00672(3)	5.02351(6)	5.04765(7)	5.0582(1)	5.2513(1)	5.29060(1)
c/Å	16.1902(2)	16.2180(3)	16.2356(4)	16.2408(7)	16.2686(5)	16.24603(6)
β/deg.	110.2065(6)	110.2554(9)	110.3460(9)	110.4008(18)	111.209(1)	111.4012(2)
V/Å^3	656.697(11)	661.903(19)	668.25(2)	671.07(4)	718.82(14)	717.16(3)
M–O(1)/Å	1.944(9)	1.983(7)	1.998(9)	1.998(12)	2.119(13)	2.085(5)
M–O(2)/Å	1.942(11)	1.960(8)	1.975(10)	1.937(16)	2.089(16)	2.090(6)
M–O(3)/Å	1.913(11)	1.874(9)	1.960(10)	1.938(16)	1.980(16)	2.086(6)
M–O(5)/Å	1.969(10)	1.978(8)	1.978(10)	1.937(15)	2.207(15)	2.084(6)
M–O(6)/Å	1.941(11)	1.969(9)	1.987(11)	1.983(17)	2.084(17)	2.105(6)
M–O(7)/Å	1.962(8)	1.988(7)	1.944(8)	1.952(11)	2.075(10)	2.090(5)
$\langle M$–O$\rangle$/Å	1.945	1.959	1.974	1.958	2.092	2.090
χ^2	3.000	3.095	2.393	2.091	3.937	2.844
R_p/%	4.93	4.52	3.90	3.98	4.04	5.51
R_{wp}/%	6.41	5.89	5.12	5.21	5.43	7.37

Table 3
Fractional atomic coordinates and isotropic thermal displacement parameters with estimated standard deviations for α-$Ti(HPO_4)_2 \cdot H_2O$ from the Rietveld refinement.

Atom	x	y	z	U_{iso} ($\times 10^2$) Å^2
Ti	0.7594(3)	0.2518(13)	0.5120(2)	0.05(4)
P(1)	−0.0046(4)	0.7448(15)	0.6073(2)	0.27(7)
P(2)	0.4671(4)	0.2454(15)	0.5992(2)	0.27(7)
O(1)	0.1151(10)	0.8276(16)	0.5643(6)	0.49(9)
O(2)	−0.0640(11)	0.4681(17)	0.5903(8)	0.49(9)
O(3)	0.8570(11)	0.9581(16)	0.5876(7)	0.49(9)
O(4)	0.0967(7)	0.7694(22)	0.7093(5)	0.49(9)
O(5)	0.3273(10)	0.4249(16)	0.5580(6)	0.49(9)
O(6)	0.4169(11)	−0.0391(17)	0.5681(7)	0.49(9)
O(7)	0.6260(10)	0.3246(17)	0.5860(5)	0.49(9)
O(8)	0.5081(7)	0.2506(25)	0.7023(5)	0.49(9)
O(9)	0.2559(9)	0.2307(18)	0.7631(5)	0.21(2)

Table 4
Fractional atomic coordinates and isotropic thermal displacement parameters with estimated standard deviations for α-$Ti_{0.9}Zr_{0.1}(HPO_4)_2 \cdot H_2O$ from the Rietveld refinement.

Atom	x	y	z	U_{iso} ($\times 10^2$) Å^2	Fractional occupancy
Ti	0.7591(2)	0.2459(9)	0.5126(1)	0.44(4)	0.911(4)
	0.7591(2)	0.2459(9)	0.5126(1)	0.44(4)	0.089(4)
P(1)	−0.0040(3)	0.7356(10)	0.6081(2)	0.06(5)	
P(2)	0.4671(3)	0.2468(11)	0.5996(2)	0.06(5)	
O(1)	0.1155(8)	0.8252(14)	0.5668(5)	0.55(7)	
O(2)	−0.0684(9)	0.4739(15)	0.5909(6)	0.55(7)	
O(3)	0.8517(9)	0.9535(15)	0.5845(6)	0.55(7)	
O(4)	1.0983(6)	0.7763(18)	0.7092(4)	0.55(7)	
O(5)	0.3238(9)	0.4257(14)	0.5557(5)	0.55(7)	
O(6)	0.4193(9)	−0.0314(15)	0.5687(6)	0.55(7)	
O(7)	0.6265(8)	0.3342(14)	0.5874(4)	0.55(7)	
O(8)	0.5088(6)	0.2463(21)	0.7022(3)	0.55(7)	
O(9)	0.2559(8)	0.2325(18)	0.7631(4)	0.36(11)	

patterns of the coprecipitates are similar to those of the end members. The products with up to 30% Zr (nominally $Ti_{0.9}Zr_{0.1}(HPO_4)_2 \cdot H_2O$, $Ti_{0.8}Zr_{0.2}(HPO_4)_2 \cdot H_2O$ and $Ti_{0.7}Zr_{0.3}(HPO_4)_2 \cdot H_2O$) give patterns similar to α-TiP and vice versa for the 90% Zr product ($Ti_{0.1}Zr_{0.9}(HPO_4)_2 \cdot H_2O$) and α- ZrP, as expected from similar findings by Clearfield and Frianeza [5]. The patterns of the other coprecipitates (nominally $Ti_{0.6}Zr_{0.4}(HPO_4)_2 \cdot H_2O$, $Ti_{0.5}Zr_{0.5}(HPO_4)_2 \cdot H_2O$, $Ti_{0.4}Zr_{0.6}(HPO_4)_2 \cdot H_2O$, $Ti_{0.3}Zr_{0.7}(HPO_4)_2 \cdot H_2O$ and $Ti_{0.2}Zr_{0.8}(HPO_4)_2 \cdot H_2O$) contain both more and broader peaks, suggesting a two phase nature.

3.2. X-ray fluorescence (XRF) measurements

The bulk elemental compositions of the mixed metal samples as determined by XRF are shown in Table 1. Good agreement is seen between the expected and the actual Zr/Ti ratios in the products that appear to be single phase by XRD. The samples in the middle of the solid solution (ca. 60–20 nominal% Ti) appear to have approximately the same bulk composition irrespective of starting Ti/Zr ratios, in all cases the solid is Ti-rich relative to the expected ratio. This suggests some aspect of the solution

Table 5
Fractional atomic coordinates and isotropic thermal displacement parameters with estimated standard deviations for α-$Ti_{0.8}Zr_{0.2}(HPO_4)_2 \cdot H_2O$ from the Rietveld refinement.

Atom	x	y	z	U_{iso} ($\times 10^2$) Å^2	Fractional occupancy
Ti	0.75906(27)	0.2483(10)	0.5124(2)	1.86(9)	0.862(4)
Zr	0.75906(27)	0.2483(10)	0.5124(2)	1.86(9)	0.138(4)
P(1)	−0.0037(4)	0.7436(15)	0.6092(2)	0.81(2)	
P(2)	0.4679(4)	0.2517(14)	0.5996(2)	0.81(2)	
O(1)	0.1132(11)	0.8204(17)	0.5666(6)	1.71(5)	
O(2)	−0.0656(11)	0.4688(18)	0.5935(7)	1.71(5)	
O(3)	0.8605(12)	0.9541(17)	0.5914(7)	1.71(5)	
O(4)	1.0959(8)	0.7180(23)	0.7083(5)	1.71(5)	
O(5)	0.3282(11)	0.4307(16)	0.5583(6)	1.71(5)	
O(6)	0.4191(12)	−0.0292(18)	0.5690(7)	1.71(5)	
O(7)	0.6325(11)	0.3307(17)	0.5870(5)	1.71(5)	
O(8)	0.5059(7)	0.2723(23)	0.7030(4)	1.71(5)	
O(9)	0.2579(11)	0.2298(25)	0.7625(5)	2.74(1)	

Table 6
Fractional atomic coordinates and isotropic thermal displacement parameters with estimated standard deviations for α-$Ti_{0.7}Zr_{0.3}(HPO_4)_2 \cdot H_2O$ from the Rietveld refinement.

Atom	x	y	z	U_{iso} ($\times 10^2$) Å^2	Fractional Occupancy
Ti	0.7576(3)	0.2527(12)	0.5126(2)	0.55(8)	0.779(6)
Zr	0.7576(3)	0.2527(12)	0.5126(2)	0.55(8)	0.221(6)
P(1)	−0.0040(6)	0.7479(21)	0.6083(3)	0.46(12)	
P(2)	0.4684(6)	0.2264(17)	0.6005(3)	0.46(12)	
O(1)	0.1110(15)	0.8123(28)	0.5645(8)	1.07(6)	
O(2)	−0.0665(18)	0.4650(27)	0.5905(9)	1.07(6)	
O(3)	0.8491(18)	0.9449(28)	0.5839(10)	1.07(6)	
O(4)	1.0967(10)	0.7516(49)	0.7072(6)	1.07(6)	
O(5)	0.3179(16)	0.4168(27)	0.5483(8)	1.07(6)	
O(6)	0.4094(18)	−0.0145(29)	0.5671(11)	1.07(6)	
O(7)	0.6287(15)	0.3342(27)	0.5865(6)	1.07(6)	
O(8)	0.5107(9)	0.2536(47)	0.7033(5)	1.07(6)	
O(9)	0.2529(16)	0.2250(39)	0.7609(7)	1.92(3)	

Table 7
Fractional atomic coordinates and isotropic thermal displacement parameters with estimated standard deviations for α- $Ti_{0.1}Zr_{0.9}(HPO_4)_2 \cdot H_2O$ from the Rietveld refinement.

Atom	x	y	z	U_{iso} ($\times 10^2$) Å^2	Fractional occupancy
Ti	0.7597(3)	0.2518(10)	0.5144(1)	0.81(9)	0.299(8)
Zr	0.7597(3)	0.2518(10)	0.5144(1)	0.81(9)	0.701(8)
P(1)	−0.0062(7)	0.7291(20)	0.6136(3)	0.22(2)	
P(2)	0.4694(6)	0.2349(21)	0.1044(3)	0.22(2)	
O(1)	0.1073(16)	0.8316(24)	0.5663(8)	0.36(7)	
O(2)	0.9407(19)	0.4801(27)	0.5990(11)	0.36(7)	
O(3)	0.8698(19)	0.9666(29)	0.5923(11)	0.36(7)	
O(4)	0.1151(11)	0.7859(33)	0.7176(6)	0.36(7)	
O(5)	0.3429(19)	0.4125(27)	0.5682(9)	0.36(7)	
O(6)	0.4103(20)	−0.0128(28)	0.5722(10)	0.36(7)	
O(7)	0.6176(13)	0.2771(35)	0.5900(6)	0.36(7)	
O(8)	0.5116(10)	0.2462(48)	0.7075(6)	0.36(7)	
O(9)	0.2519(19)	0.2373(46)	0.7564(8)	3.26(13)	

chemistry influences the products that form, irrespective of whether or not the structure type is able to accommodate a full solid solution between the end member compositions.

3.3. Rietveld refinements

Rietveld profile analysis was undertaken on all solids using high resolution synchrotron X-ray data. Those samples deemed to be single phase from laboratory data could be successfully refined as such starting from the structure for α-TiP as given by Salvado et al. [19] using space group $P2_1/c$. For the mixed metal samples the compositions were allowed to refine starting from the values expected from the nominal compositions, but fractional occupancies were constrained to sum to 1. During the refinements the temperature factors of each discrete atom type were constrained to the same value, excluding that for the water oxygen, O(9), which was refined independently. A summary of key structural parameters is presented in Table 2, details of atomic coordinates and thermal parameters in Tables 3–8 and fits to the data shown in Fig. 3 and Appendix A. The refined parameters for the end members are in excellent agreement with those in the literature [19,20].

Table 8
Fractional atomic coordinates and isotropic thermal displacement parameters with estimated standard deviations for α- $Zr(HPO_4)_2 \cdot H_2O$ from the Rietveld refinement.

atom	x	y	z	U_{iso} ($\times 10^2$) Å^2
Zr	0.7612(1)	0.2531(4)	0.51476(5)	1.44(1)
P(1)	0.0007(2)	0.7483(10)	0.6141(1)	0.705(7)
P(2)	0.4697(2)	0.2580(9)	0.1038(1)	0.705(7)
O(1)	0.1057(6)	0.8018(10)	0.5646(3)	0.98(4)
O(2)	0.9364(7)	0.4870(11)	0.6001(4)	0.98(4)
O(3)	0.8715(7)	0.9471(10)	0.5944(4)	0.98(4)
O(4)	0.1049(5)	0.7743(13)	0.7146(3)	0.98(4)
O(5)	0.3460(7)	0.4324(10)	0.5606(4)	0.98(4)
O(6)	0.4147(7)	−0.0155(11)	0.5705(4)	0.98(4)
O(7)	0.6226(6)	0.3090(10)	0.5916(2)	0.98(4)
O(8)	0.5065(4)	0.2396(18)	0.7048(3)	0.98(4)
O(9)	0.2579(6)	0.2245(13)	0.7632(3)	1.75(9)

Various plots for selected unit cell parameters and mean metal–oxygen distances are shown in Fig. 4. The variation in the monoclinic angle is not shown, but it is clear from the data in Table 2 that it varies in a similar, yet much less dramatic, fashion. As expected, all of these increase with the content of the larger Zr ion. The fact that the a- and b-axis are much more sensitive to metal content is readily explained by the layers and most of the M–O bonds being in the a,b-plane. Nearly all of the volume expansion when moving from Ti to Zr is due to these as the interplanar spacing, approximately along the c-axis, is the same for the end members at 7.56 Å. In the graphs there are two lines. One of these connects the values for the end members and therefore if the mixed samples obeyed Vegard's Law one would expect their values to fall on the line. In each graph a second line is drawn based on a least-squares fit to the 4 points for the Ti end-member samples. These all have a smaller gradient than expected, which may be a significant indicator that the introduction of the larger Zr ion strains the system and may be an underlying feature preventing the formation of the full range of solid solutions.

The samples with $x=0.4$–0.8 gave complex patterns and had to be treated as two-phase mixtures. Given the similarities of the powder patterns of the two phases and therefore extreme overlap in each data set, it was not possible to refine metal site occupancies and obtain sensible values. In all cases, based on the linear extrapolation of the unit cell values between the end members, one phase had a composition close to 14% Ti and the other approximately 68% Ti, therefore the compositions were fixed at these values and phase fractions refined. The results of the fits are summarised in Table 9 and a representative plot is shown in Fig. 5. Compositions as determined from Rietveld and XRF analyses are compared in Table 10 and are discussed later in the paper.

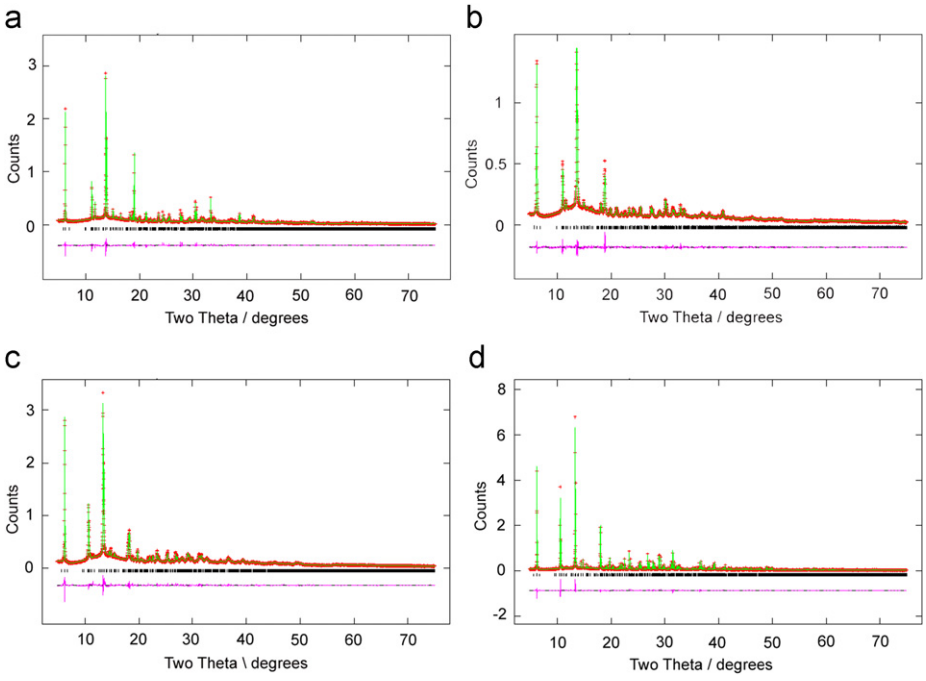

Fig. 3. Final observed (red crosses), calculated (green line) and difference (bottom) X-ray diffraction profiles with reflection positions noted as vertical tick marks for: (a) α-$Ti(HPO_4)_2 \cdot H_2O$, (b) α-$Ti_{0.7}Zr_{0.3}(HPO_4)_2 \cdot H_2O$, (c) α-$Ti_{0.1}Zr_{0.9}(HPO_4)_2 \cdot H_2O$ and (d) α-$Zr(HPO_4)_2 \cdot H_2O$. (For interpretation of the references to colour in this figure legend, the reader is referred to the web version of this article.)

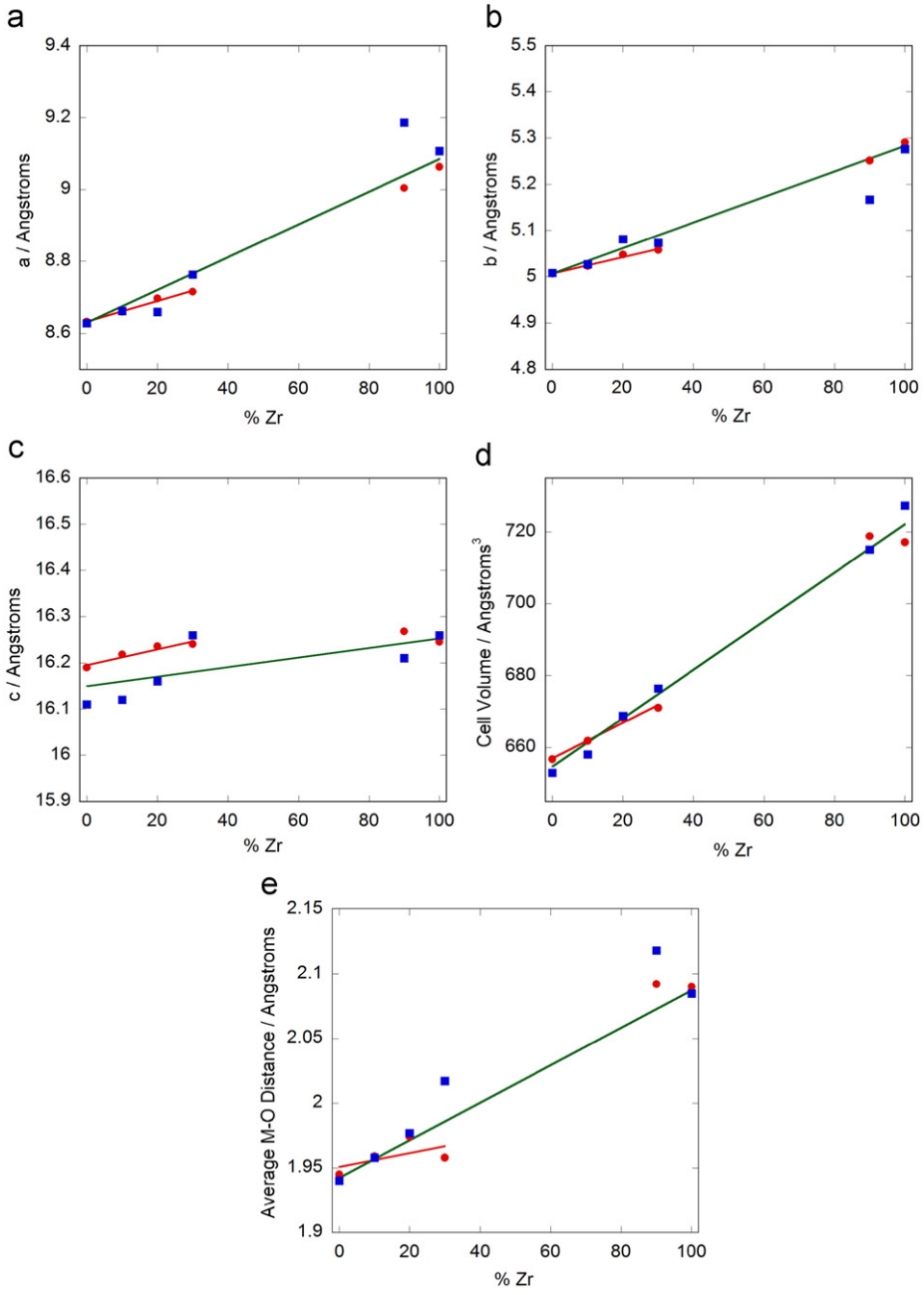

Fig. 4. Unit cell parameters for: (a) *a*-axis; (b) *b*-axis; (c) *c*-axis; (d) volume and (e) mean *M*–O distance versus %Zr for the single-phase compositions in the Zr/Ti series. Red circles are data from the Rietveld refinements and blue squares from the PDF fits. The green lines connect the average values from the end members, the red lines are best fits for the Rietveld points at the Ti-rich end. (For interpretation of the references to colour in this figure legend, the reader is referred to the web version of this article.)

Table 9
Structural parameters for the two phase products from the Rietveld refinements.

	$Ti_{0.6}Zr_{0.4}(HPO_4)_2 \cdot H_2O$		$Ti_{0.5}Zr_{0.5}(HPO_4)_2 \cdot H_2O$		$Ti_{0.4}Zr_{0.6}(HPO_4)_2 \cdot H_2O$		$Ti_{0.3}Zr_{0.7}(HPO_4)_2 \cdot H_2O$		$Ti_{0.2}Zr_{0.8}(HPO_4)_2 \cdot H_2O$	
Space group	Phase 1 $P2_1/c$	Phase 2 $P2_1/c$	Phase 1 $P2_1/c$	Phase 2 $P2_1/c$	Phase 1 $P2_1/c$	Phase 2 $P2_1/c$	Phase 1 $P2_1/c$	Phase 2 $P2_1/c$	Phase 1 $P2_1/c$	Phase 2 $P2_1/c$
a/Å	9.0091(6)	8.7150(4)	9.0168(8)	8.7161(6)	9.0207(2)	8.7190(5)	9.0161(2)	8.7238(6)	9.0198(2)	8.7354(12)
b/Å	5.2549(3)	5.06319(23)	5.2588(4)	5.0640(3)	5.26187(14)	5.06420(27)	5.25866(9)	5.0659(3)	5.2608(1)	5.0697(7)
c/Å	16.2444(10)	16.2424(10)	16.2482(16)	16.2451(15)	16.2561(4)	16.2533(11)	16.2597(3)	16.2485(8)	16.2661(4)	16.2756(17)
β/deg	111.273(3)	110.422(3)	111.285(5)	110.420(4)	111.274(1)	110.417(3)	111.265(9)	110.414(4)	111.268(1)	110.376(7)
V/Å^3	716.64(8)	671.66(6)	717.90(11)	671.97(9)	719.03(3)	672.58(7)	718.43(2)	672.98(7)	719.29(3)	675.50(13)
$<$M-O$>$/Å	2.19	2.02	1.90	2.07	2.15	1.98	2.15	2.02	2.13	2.03
Ti Frac.	0.14	0.68	0.14	0.68	0.14	0.68	0.14	0.68	0.14	0.68
Zr Frac.	0.86	0.32	0.86	0.32	0.86	0.32	0.86	0.32	0.86	0.32
Weight frac.	21%	79%	23%	77%	55%	45%	64%	36%	72%	28%

3.4. Pair distribution function (PDF) studies

Fig. 6 shows the overlaid PDF patterns for the full series of mixed Zr/Ti phosphates for the low-*r* region, with the intensities scaled on the phosphorous–oxygen peak height which must remain constant. Each peak represents different atomic distances present in the structure so that variation in bond lengths can be easily seen. By inspection, it is clear that the Ti based products do have smaller intralayer interatomic distances, as shown by the oxygen–oxygen, phosphorous–phosphorous, metal–oxygen and metal–metal peaks at approximately 3.44, 4.44, 2.05 and 5.00–5.50 Å, respectively. It is worth highlighting that these distances can be taken directly from the PDF patterns, i.e. no analysis of atomic coordinates and unit cell parameters is required. It is also interesting to observe that the *M*–O peak distance changes little with doping, i.e. the Ti-rich samples all have an average distance similar to α-TiP and the Zr-rich samples all have an average distance similar to α-ZrP. This is not as one would naturally expect for a normal solid solution where a smoothly changing *M*–O distance would be predicted. Another aspect readily apparent upon close inspection of the intraplanar *M*–*M* peak, Fig. 7, is that the systems that could be analysed using the Rietveld method have a single peak whereas the two-phase samples show the expected two peaks. The observation from the PDF patterns, in the absence of knowledge from the Rietveld analysis, could only be explained by phase segregation or a lowering of the crystallographic symmetry.

A particular strength of the PDF method is that it should be more powerful than Rietveld analysis for determining the distribution of metals in solid solutions. There are three possible types of metal ordering within these systems: complete random disorder, local clustering and phase segregation in large domains as depicted in Fig. 8. PDF can distinguish between these by, for example, studying in detail the *M*–*M* peaks and in the case of clustering determine the length scale. If the products were two-phase then one would expect to see two separate peaks in the region of 5 Å, reflecting the presence of both Zr–Zr and Ti–Ti distances. Single phase products with no metal ordering are expected to display a single peak, varying in

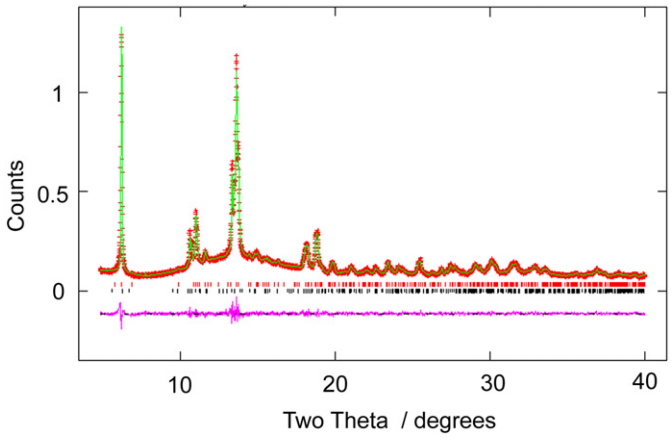

Fig. 5. Final observed (red crosses), calculated (green line) and difference (bottom) X-Ray profiles for α- $Ti_{0.5}Zr_{0.5}(HPO_4)_2 \cdot H_2O$ with reflection positions noted as vertical tick marks (phase one shown in black and phase two in red.). (For interpretation of the references to colour in this figure legend, the reader is referred to the web version of this article.)

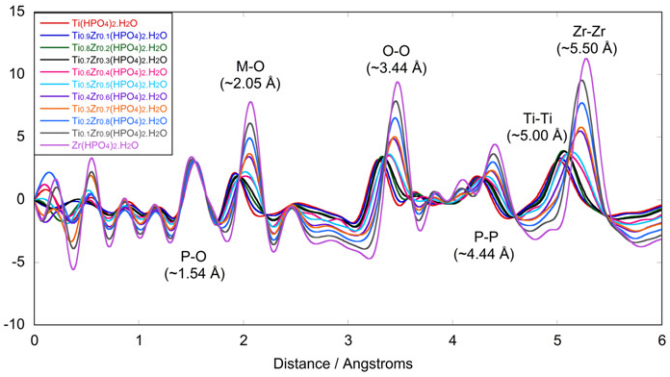

Fig. 6. PDF patterns for the series.

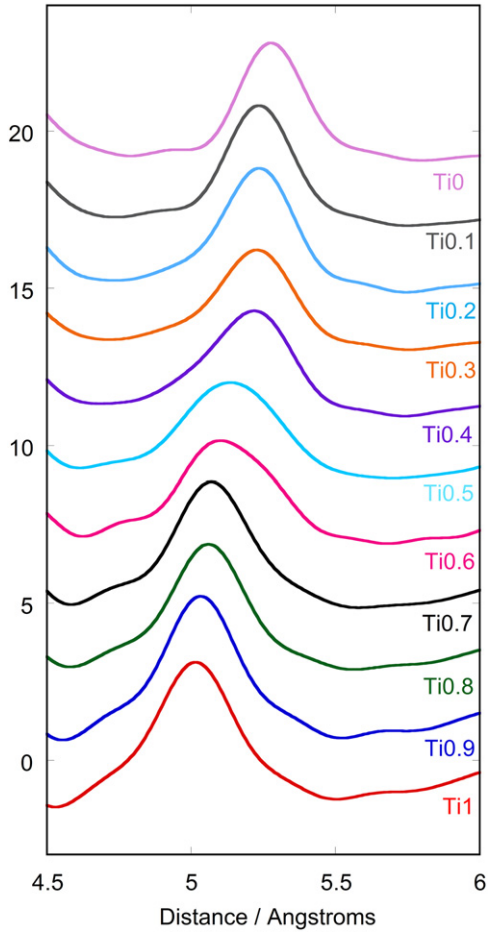

Fig. 7. PDF patterns of the region where metal–metal peaks are observed.

Table 10
Comparison of compositions as determined from Rietveld and XRF analyses for the two-phase samples.

Nominal product	Ti (Rietveld)	Zr (Rietveld)	Ti/Zr ratio Rietveld	Ti/Zr ratio XRF	Expected Ti/Zr ratio
$Ti_{0.6}Zr_{0.4}(HPO_4)_2 \cdot H_2O$	0.567	0.433	1.31	1.22	1.50
$Ti_{0.5}Zr_{0.5}(HPO_4)_2 \cdot H_2O$	0.556	0.444	1.25	1.13	1.00
$Ti_{0.4}Zr_{0.6}(HPO_4)_2 \cdot H_2O$	0.383	0.617	0.62	0.92	0.67
$Ti_{0.3}Zr_{0.7}(HPO_4)_2 \cdot H_2O$	0.334	0.665	0.50	0.85	0.43
$Ti_{0.2}Zr_{0.8}(HPO_4)_2 \cdot H_2O$	0.291	0.709	0.25	0.85	0.25

distance throughout the series but a clustering of metal atoms is expected to produce at least three peaks (representing Zr–Zr, Ti–Ti and Zr–Ti distances). An inspection of the metal–metal peak region in the PDF patterns for the whole series (Fig. 7) is indicative that the solid solutions with $x=0.1$, 0.2, 0.3 or 0.9 have a random distribution of the metal atoms within the layers, rather than clustering. This is evident from the presence of one peak with a smoothly changing *M–M* distance. These findings are in contrast to those reported by Farfan-Torres et al. [11] where it was indicated that there was a hexagonal distribution of the metal atoms within the planes of the solid solutions formed. The only evidence given to support this hypothesis was the metal ratios of the products believed from XRD to be single phase. Rietveld refinements do not provide such information about the metal ordering within structures.

3.5. PDF refinements

All of the PDFs for the single phase materials were modelled using PDFGui. The starting models were as noted for the Rietveld work and metal fractions refined. The fits were excellent, with R_{wp} values of 0.084, 0.058, 0.061, 0.066, 0.108 and 0.065 for $x=0$, 0.1, 0.2, 0.3, 0.9 and 1, respectively. A summary of unit cell parameters and selected bond distances are given along with a comparison to those derived from the Rietveld refinements in Table 11. Fits to the data and crystallographic details can be found in Appendix A. Even though these materials are crystallographically relatively complex compared to other systems studied using PDF in the literature, the correspondence of refined unit cells and atomic parameters with the more conventional Rietveld analysis are very good. Due to the nature of the PDF method, which is giving real space information regarding neighbouring atoms, it is expected that PDF refinements will provide more accurate average bond distances whereas a Rietveld analysis is better employed in the determination of accurate unit cell parameters. We are, unfortunately, unable to calculate accurate estimated standard deviations on the derived parameters as the data were collected using an area detector and the integration software, FIT2D, does not produce estimated standard deviations on the individual data points.

3.6. Limits of the solid solution

Our findings further support the idea that the saturation point of Zr within α-TiP is around 30% and Ti in α-ZrP is around 10%

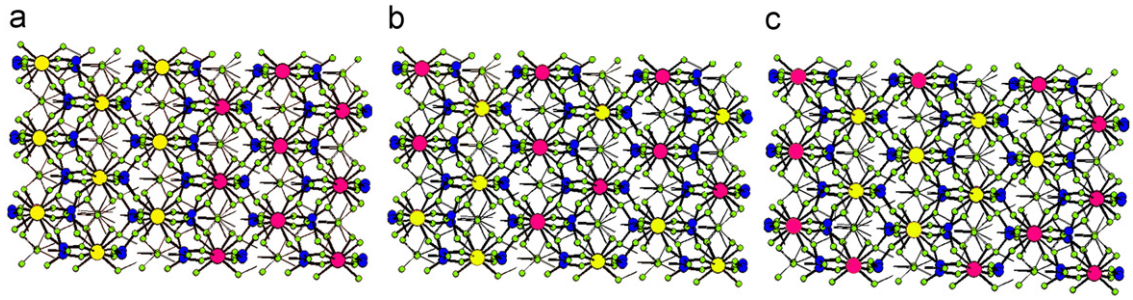

Fig. 8. Possible metal distributions: (a) phase segregation, (b) random disorder and (c) clustering where Ti atoms are pink and Zr are yellow. (For interpretation of the references to colour in this figure legend, the reader is referred to the web version of this article.)

Table 11
Comparison of refined unit cell parameters and metal–oxygen distances for the single-phase members of the series, PDF derived numbers are in normal font and those from Rietveld analysis are shown in italics for comparison. The esd's on the numbers from the PDF analysis are undetermined as esd's on the individual data points are unknown.

	α- TiP	α- $Ti_{0.9}Zr_{0.1}(HPO_4)_2.H_2O$	α- $Ti_{0.8}Zr_{0.2}(HPO_4)_2 \cdot H_2O$	α- $Ti_{0.7}Zr_{0.3}(HPO_4)_2 \cdot H_2O$	α- $Ti_{0.1}Zr_{0.9}(HPO_4)_2 \cdot H_2O$	α- ZrP
a/Å	8.628	8.662	8.659	8.763	9.186	9.107
	8.63267(6)	*8.65991(12)*	*8.69672(13)*	*8.7156(3)*	*9.0048(2)*	*9.06336(2)*
b/Å	5.008	5.027	5.081	5.073	5.167	5.276
	5.00672(3)	*5.02351(6)*	*5.04765(7)*	*5.0582 (1)*	*5.2513(1)*	*5.29060(1)*
c/Å	16.11	16.12	16.16	16.26	16.21	16.26
	16.19025(24)	*16.21800(34)*	*16.23560(35)*	*16.2408(7)*	*16.2680(5)*	*16.24603(6)*
β/°	110.26	110.34	109.85	110.69	111.63	111.42
	110.2065(6)	*110.2554(9)*	*110.3460(9)*	*110.4008(18)*	*111.2093(13)*	*111.40120(2)*
V/Å^3	652.91	658.08	668.84	676.42	715.07	727.31
	656.697(11)	*661.90(2)*	*668.25(2)*	*671.07(4)*	*718.82(14)*	*717.16(3)*
M-O(1)/Å	2.014	1.854	2.046	1.948	1.918	2.240
	1.944(9)	*1.983(7)*	*1.998(9)*	*1.998(12)*	*2.119(13)*	*2.083(5)*
M-O(2)/Å	1.913	2.002	2.097	1.939	2.472	1.985
	1.942(11)	*1.960(8)*	*1.975(10)*	*1.937(16)*	*2.089(16)*	*2.090(6)*
M-O(3)/Å	1.899	1.961	1.853	1.929	2.092	2.100
	1.913(11)	*1.874(9)*	*1.960(10)*	*1.938(16)*	*1.980(16)*	*2.086(6)*
M-O(5)/Å	1.918	2.095	1.986	2.117	2.009	2.082
	1.969(10)	*1.978(8)*	*1.978(10)*	*1.937(15)*	*2.207(15)*	*2.084(6)*
M-O(6)/Å	2.024	1.907	1.924	2.041	2.093	2.096
	1.941(11)	*1.969(9)*	*1.987(11)*	*1.983(17)*	*2.084(17)*	*2.105(6)*
M-O(7)/Å	1.875	1.931	1.956	2.126	2.126	2.009
	1.962(8)	*1.988(7)*	*1.944(8)*	*1.952(11)*	*2.075(10)*	*2.090(5)*
< M-O > /Å	1.940	1.958	1.977	2.017	2.118	2.085
	1.945	1.959	1.974	1.958	2.092	2.090

even though the end members are isostructural. This differs slightly from previous findings [11] where it was believed that both unit cells could withstand 25% metal substitution but not 33%. This is in spite of the fact that we have employed yet another crystallisation method that, in our experience, is far superior to those in the literature for the end members. The exact reason for the lack of a solid solution remains unclear. It is interesting to note that the average *M*–O distance does not seem to vary much from the end member values when the second metal is accommodated, so it may be that the unit cells cannot withstand the alterations that are required in the *a*- and *b*-directions to accommodate more of the second metal. It should also be noted that it is obvious that in all of the two-phase systems there is a much larger amorphous component in the powder diffraction patterns, indicative of a frustrated system so perhaps one that is unable to crystallise under the relatively mild conditions employed. The Rietveld analysis of the mixed phase systems shows the compositions of the crystalline components sum (based on the weight fractions) to close to the expected ratios of Ti and Zr, Table 10. The XRF measurements, however, show the overall bulk solid compositions in this range are nearly the same at ca. 50% Ti, Table 1. This discrepancy must be due to the amorphous components which would seem to be Zr-rich for the nominal 60% Ti system and Ti-rich for the other four. This is in keeping with an XRF measurement of the filtrate from the 50:50 synthesis mixture, where the molar ratio of Ti to Zr in solution of 0.6 is less than the starting value of 1.0 and shows that there is an excess of Zr that remains. The full answer may therefore be more complicated than just lattice strain, and involve aspects of the solution chemistry, nature of the amorphous pre-cursor(s) from which the layered phosphates crystallise and relative rates of crystallisation under the mild hydrothermal conditions employed.

4. Conclusion

In conclusion it can be stated that α-zirconium and titanium phosphates form solid solutions with each other, but in keeping with reports using other crystallisation routes there is a miscibility gap. The solid solutions high in zirconium behave as zirconium phosphate and vice versa for those with high titanium contents. This includes the average *M*–O distance, which does not seem to change in a linear fashion between the end members. PDF analysis indicates there is no metal ordering within these compounds in contrast to previous suggestions.

Acknowledgments

This work was financially supported by EPSRC and the University of Birmingham, and carried out with the support of Diamond Light Source. We wish to thank Peter Chupas and Karena Chapman at the APS for help with the PDF measurements and work. Use of the APS was supported by the US DOE, Office of Basic Energy Sciences, through contract No. DEAC02-06CH11357. The Bruker S8 system used in this research was obtained, through the Science City Advanced Materials project: Creating and Characterising Next Generation Advanced Materials project, with support from Advantage West Midlands (AWM) and part funded by the European Regional Development Fund (ERDF).

Appendix A. Supplementary material

Supplementary data associated with this article can be found in the online version at doi:10.1016/j.jssc.2010.07.028.

References

[1] G. Alberti, P. Cardini-Galli, U. Costantino, E. Torracca, J. Inorg. Nucl. Chem. 29 (1967) 571–578.
[2] A. Clearfield, in: Inorganic Ion Exchange Materials, CRC Press, Boca Raton, FL, 1982.
[3] R. Llavona, M. Suarez, J.R. Garcia, J. Rodriguez, Inorg. Chem. 28 (1989) 2863–2868.
[4] A. Nilchi, M. Ghanadi Maragheh, A. Khanchi, M.A. Farajzadeh, A.A. Aghaei, J. Radio Nucl. Chem. 261 (2004) 393–400.
[5] A. Clearfield, T.N. Frianeza, J. Inorg. Nucl. Chem. 40 (1978) 1925–1932.
[6] A. Clearfield, W.L. Duax, A.S. Medina, G.D. Smith, J.R. Thomas, J. Phys. Chem. 73 (1969) 3424–3430.
[7] V.A. Winkler, E. Thilo, Z. Anorg. Allg. Chem. 364 (1966) 92–112.
[8] U. Costantino, A. Gasperoni, J. Chromatogr. 51 (1970) 289–296.
[9] L. Peters, J.S.O. Evans, J. Solid State Chem. 180 (2007) 2363–2370.
[10] A. Clearfield, G.D. Smith, Inorg. Chem. 8 (1969) 431–436.
[11] E.M. Farfan-Torres, E.L. Sham, M. Martinez-Lara, A. Jimenez-Lopez, Mater. Res. Bull. 27 (1992) 1255–1262.
[12] L. Szirtes, Z. Poko, S.K. Shakshooki, M. Ahmed, A. Dehair, A. Benhamed, J. Therm. Anal. 35 (1989) 895–902.
[13] S.P. Thompson, J.E. Parker, J. Potter, T.P. Hill, A. Birt, T.M. Cobb, Y. Yuan, C.C. Tang, Rev. Sci. Instrum. 80 (2009) 075107–075109.
[14] C.C. Tang, S.P. Thompson, T.P. Hill, G.R. Wilkin, U.H. Wagner, Z. Kristallogr. Suppl. 26 (2007) 153–158.
[15] A. Larson, R.B. von Dreele, GSAS: Generalized Structure Analysis System, Report No. L.A-UR-86-748: LANSCE, Los Alamos National Laboratory, Los Alamos, NM, 1985.
[16] A.P. Hammersley, Syn. Rad. News 2 (1989) 24–26.
[17] X. Qui, W. Thompson, S.J.L. Billinge, J. Appl. Cryst. 37 (2004) 678.
[18] C.L. Farrow, P. Juhas, J.W. Liu, J. Phys.: Condens. Matter 19 (2007) 1–7.
[19] M.A. Salvado, P. Pertierra, S. Garcia-Granda, J.R. Garcia, J. Rodriguez, M.T. Fernandez-Diaz, Acta Cryst. B52 (1996) 896–898.
[20] J.M. Troup, A. Clearfield, Inorg. Chem. 16 (1977) 3311–3313.